Energy and Buildings 160 (2018) 34–43

Contents lists available at ScienceDirect

Energy and Buildings

journal homepage: www.elsevier.com/locate/enbuild

Development of moisture absorber based on hydrophilic nonporous membrane mass exchanger and alkoxylated siloxane liquid desiccant

Jovan Pantelic[a,b,d], Eric Teitelbaum[a,b,c], Michael Bozlar[a,b], Soram Kim[a], Forrest Meggers[a,b,c,*]

[a] School of Architecture, Princeton University, United States
[b] Andlinger Center for Energy and the Environment, Princeton University, United States
[c] Department of Civil and Environmental Engineering, Princeton University, Princeton, NJ 08544, United States
[d] Eidgenössische Technische Hochschule (ETH) Zürich, Department of Architecture, Institute of Technology in Architecture, Switzerland

ARTICLE INFO

Article history:
Received 30 November 2016
Received in revised form 9 October 2017
Accepted 30 October 2017
Available online 21 November 2017

Keywords:
Liquid desiccant
Hydrophilic nonporous membrane
Absorber
Dehumidification

ABSTRACT

In order to deal with corrosion, crossover and desiccant utilization issues encountered in commercially available liquid desiccant systems, we develop and characterize the performance of a hydrophilic nonporous membrane-based liquid desiccant absorber. The liquid desiccant is an alkoxylated siloxane mixture, a modified silicone oil for enhanced moisture absorption. Performance is characterized for a shell and tube configuration by measuring air temperature and relative humidity at the inlet and outlet of the absorber. We determine the characteristics of counter and parallel flow configurations, various air and liquid desiccant flow rates and several contact lengths within the membrane absorber. The absorption was weakly increased by liquid desiccant flow rate. Results for counterflow configuration show that the humidity ratio of the air entering the membrane system can be reduced by up to 15.7 g/kg at maximum air flow Re number and longest contact length. Desiccant utilization in the system ranged up to 0.012 g of water per gram of desiccant. The highest desiccant utilization does not correspond to the highest mass flux rate, suggesting that the most effective system does not depend on on the quantity of removal, but rather the rate. Bulk diffusion of moisture into the desiccant is the rate limiting step for moisture absorption, with with five times faster absorption in the first 10 cm of contact length, guiding us toward future system design.

1. Introduction

Cooling buildings is a technical feat that while only being achieved a century ago, has now become ubiquitous. Effective cooling of a building requires in particular proper handling of moisture level, and many of the largest developing cities are located in hot and humid tropical climates. Humidity in indoor environments has an impact on thermal comfort [16], productivity [25] and occupant health [3]. Apart from regions with desert climates, annual latent ventilation loads are several times greater than sensible loads for HVAC [9]. Due to these high latent loads, effective and efficient dehumidification of ventilation air is very important from an energy perspective. The most frequently used method for dehumidification is on-coil condensation that wastes cooling potential [14], and often requires reheating the air after cooling it below the dew point to mechanically remove moisture. With plenty of refrigeration capacity and cheap energy, mechanical condensation of water on cooling-coils became the defacto the method to condition air to comfortable humidity levels. Nowadays, we face energy and climate challenges that drive us to better control and reduce the energy and refrigeration use in buildings.

Desiccants offer a chemical alternative to mechanical condensation by using thermodynamically spontaneous absorption as a means to dehumidify supply air, and heat to release the chemically absorbed moisture to exhaust air, and therefore avoid extra cold condensing temperatures. Desiccant chemicals may be employed in either solid or liquid forms. Each form of desiccant is known to have drawbacks such as: physical transport limitations in solids, risk of corrosion, and evaporation in liquids [13]. Solid desiccant wheels are an efficient dehumidification alternative [12], where the electrical energy used in conventional chillers to generate subcooling for condensation can be replaced with heat or recovered dry exhaust air to regenerate a solid desiccant wheel that can absorb

* Corresponding author at: School of Architecture, Princeton University, Princeton, NJ 08544, United States.
E-mail address: fmeggers@princeton.edu (F. Meggers).

https://doi.org/10.1016/j.enbuild.2017.10.093
0378-7788/© 2017 Published by Elsevier B.V.

moisture. On the other hand, we have recently shown that liquid desiccants have the potential to allow decentralized dehumidification in buildings [14]. Liquid desiccants that must be in direct contact with air streams are commercially available, but due to their intrinsic properties, they are less popular than solid desiccant wheel systems. Liquid desiccants are commonly divided into two categories: halide salts and glycols. Halide salts are very strong desiccants, but also corrosive to most metals, hence corrosion-resistant parts, e.g. titanium, have to be used [13]. Glycols are not corrosive but highly volatile, therefore, glycol-based setups require frequent maintenance to compensate for losses. Additionally, the ability to absorb water vapor from the airstream is reduced [1] at elevated temperatures. This has important consequences for dehumidification, since the regeneration of the liquid desiccant requires additional energy in the form of heat to increase desiccant temperature, so that it can desorb water.

Current modes of humidity absorber configurations involve direct contact of liquid desiccant with the air supplied to the indoor environment. This can cause carryover of liquid droplets into the airstream [10], and can have harmful consequences to occupant health, building structure and materials [10]. Recently, membrane based desiccant systems have been developed to physically segregate the liquid desiccant and the gas phase, and ultimately overcome carryover problems [10]. Polymeric membranes provide resistance to water vapor transport from the air–liquid desiccant interface. Thus, current research is directed towards developing membranes that can minimize resistance to mass transfer, while preventing droplet carryover. The efficiencies of hydrophobic [4–6,11,28] and hydrophilic [12,21,22,30] microporous membranes have been studied in the literature, and it has been demonstrated that they do not provide complete separation between desiccant and air, if the partial pressure difference between the two streams is not well controlled. Consequently, some crossover may still take place in such a system [27]. In order to achieve complete phase separation, a nonporous membrane must be used.

In this study, we investigate a novel liquid desiccant system combined with a nonporous vapor transport membrane that minimizes contamination risks. We address the major challenges mentioned above simultaneously, namely the problems associated with diffusion of water vapor through the membrane, carryover, and corrosion. We develop a novel membrane-based liquid desiccant absorber that uses a hydrophilic nonporous membrane and an alkoxylated siloxane liquid desiccant [2] that is not corrosive nor highly volatile. We test the basic desiccant kinetics, compare the membrane/desiccant water removal rates, and analyze their interactions. We characterize the humidity control potential of this system in a variety of desiccant and airflow configurations for a single shell and tube configuration. Finally, we perform a variety of tests with different tube geometries, flow rates, and humidity levels for both shell and tube mass exchanger setups. The results suggest potential development into a larger multi-tube dehumidification system.

Using a system such as a liquid desiccant dehumidification allows for separate treatment of latent and sensible loads, as the two loads are conventionally linked due to the nature of mechanical on-coil condensation for latent load handling. By separating the loads, more flexible navigation of the psychrometric chart is possible, and cold temperatures can be used at a high temperature for radiant cooling, rather than for low temperature air cooling and dehumidification. Dehumidification technology is if cooling is handled primarily with radiant or passive chilled beams, as dried air is essential for avoiding condensation. Desiccant technology therefore enables high temperature systems for the most effective low exergy cooling strategy.

2. Materials and methods

In order to simultaneously address the limitations mentioned above, we combine a hydrophilic nonporous membrane and an alkoxylated siloxane type III liquid desiccant [2,15]. The study contains two sections, as shown in Fig. 1. Testing of the component characteristics, namely the kinetics of the liquid desiccant and the membrane was the initial characterization work [18]. Once the first part was completed, water removal rates from air flowing along a small membrane tube containing flowing desiccant were studied to understand the system dynamics. As shown in Fig. 1, the different system configurations include geometry, flow rate, and humidity ratio modulation.

2.1. Instrumentation

The weight of desiccant and other compounds were measured using a Denver Instrument S-4002 type scale (accuracy of ±0.01 g). Air temperature (T) and relative humidity (%RH) were measured using a Sensirion SHT75 type sensor. T and %RH were measured every 5 s, with accuracies of ±0.3 °C and ±1.8%RH, respectively. Airflow was measured using a Sensirion SFM 4100 type gas flow meter, with an accuracy of 0.15% of full scale or 3% of reading, whichever is dominant. Sensors were connected to an Arduino Uno board and data were recorded on a computer through the Sensirion software and a serial monitor.

Various air T and %RH combination experiments were conditioned in a cubic box with dimensions of 1 m^3. One side of the box was made of acrylic, and the rest out of plywood. Air T was regulated with an electrical heater placed inside the box and %RH with an ultrasonic humidifier (Tao Tronic) with built-in water purifier and control sensor. A fan was used to mix the air in the box. The ultrasonic humidifier had cyclic operations, and output RH was cycled by 5%. The temperature in the box reached steady state within an hour, after which air was used in experiments.

2.2. Liquid desiccant

The liquid desiccant is an alkoxylated siloxane (Dow Corning XX-8810) with a significantly reduced vapor pressure dependence on temperature. We experimentally determined the volatile content to be approximately 1–3 wt%, by drying a known amount in a vacuum-oven for 6 h under vacuum of 100 kPa and temperature of 50 °C. These alkoxylated siloxanes have good affinity for water, with the equilibrium saturation ranging between 1 and 3 wt% for 20–80 %RH in a wide range of temperatures. While this is a modest equilibrium concentration range compared to other desiccants, the range lends itself well to a mass concentration based desorption process, with minimal enthalpic input. As provided by the manufacturer, the dynamic zero shear viscosity of the neat liquid desiccant at 25 °C is 0.031 Pa s. This value compares favorably to other aqueous liquid desiccants, such as $CaCl_2$ η=0.033 Pa s at 51.32 wt%, and LiCl η=0.00989 Pa s at 41.5 wt% [26]. Additional physical properties of the alkoxylated siloxane are available in the Supplemental Material file.

2.3. Hydrophilic nonporous membrane

The shell portion of the mass and heat exchanger is a high permeability Pebax® 1074 membrane. In the following, we will refer to it as "Pebax®". The membrane material, developed by Arkema and manufactured into 1.5 mm outer diameter tubes by Foster Corporation, is a polyether block amide copolymer elastomer. The water vapor transport rate in Pebax® is controlled by the relative composition of the polyether and polyamide elements. The contact angle with the raw polymer and liquid water is about 70°, and

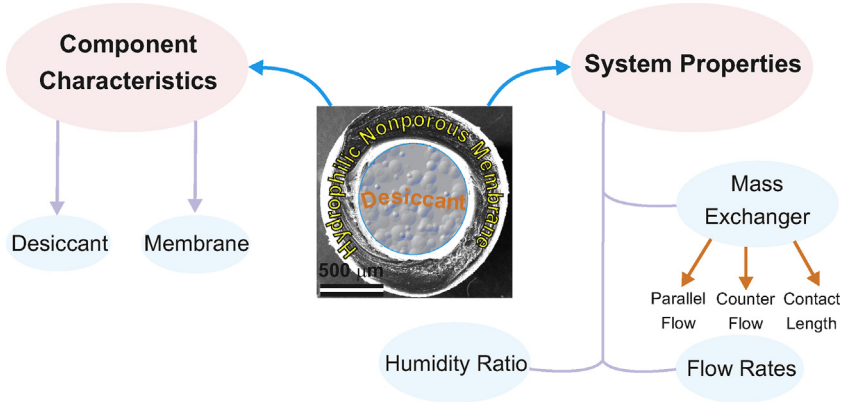

Fig. 1. Overview of experimental procedures for component characterization and system design. The scanning electron microscopy image in the center represents a cross-sectional view of the Pebax® polymeric membrane.

the pervaporation rate is reported maximally as 85 kg/m^2/day [23]. Water is transported by a solution-diffusion mechanism whereby the water or water–vapor first dissolves, and then diffuses through the membrane [19]. The membrane is impermeable to the desiccant, and diffusion of the desiccant through the membrane and into the air stream is restricted. Such a nonporous material is beneficial in environments where the desiccant must be restricted from the air stream. Because of the particularly low surface tension of the desiccant, nonporous membranes are desirable as the low surface tension could allow desiccant transport through pores, providing a crossover mechanism to the air stream. Although the membrane is hydrophilic, for neat, unsaturated desiccant with water, the partial pressure gradient is the driving force for diffusion, transporting water from the membrane into the desiccant. This simple mechanism allows moisture to energetically favor the desiccant over the membrane, eventually bringing the system into a lower energy state when water is preferably absorbed by the desiccant, compared to the membrane. Additionally, proof of concept experiments demonstrate that the rate of absorption onto free surface of quiescent liquid desiccant is an order of magnitude slower than the rate of mass transfer of water through the membrane [18,24]. The interaction potential and slower mass transfer demonstrate a shell and tube exchanger in which the wall materials do not impede transfer.

The weight of the 67 cm long Pebax® membrane was measured prior to placing the membrane inside the conditioning box, at $T = 24\,^{\circ}$C and RH of 40%. The membrane was in the conditioning box for 2 h before it reached steady state. After 2 h, the weight of the membrane was measured to determine how much water the membrane absorbed under various conditions. Experiments were repeated for T of 25, 28, and 32 °C, and RH of 60, 80, and 95%. This was needed to account for water uptake in the membrane, and to determine the time needed to ensure it was at equilibrium before measurements were made on the desiccant.

2.4. Air-desiccant exchanger experimental setup

The absorber had a tube in a shell structure. The inner tube was a Pebax® membrane tube with an outer diameter of 1.5 mm, and the outer shell consisted of Tygon tubes. The maximum length of the absorber was 67.5 cm. Three diameters of Tygon tubes were used: 3.2, 6.4, and 7.9 mm. These tubes correspond to 1/8″, 1/4″, and 5/16″ nominal Tygon tubing, respectively. However, these nominal sizes do not directly translate to actual dimensions, so for calculation purposes the actual dimensions are reported throughout this paper in mm. The liquid desiccant was pumped into the 1.5 mm outer diameter inner membrane tube inside the Tygon tube through which air was pumped, creating the shell in tube mass exchanger. Dry desiccant was supplied to the Pebax® tube from a reservoir with a peristaltic pump, items 8 and 2, respectively, in Fig. 2. The tube connecting liquid desiccant reservoir and the Pebax® membrane had a manual valve. A pump (item 9) was used to supply the air through the space between the membrane outer surface and the inner surface of the shell. In order to control the airflow rate, the air loop had a bypass with the valve that returns excess air into the conditioning box (item 10). The main air supply line had an additional valve. Before entering the shell fraction, a T and RH sensor (item 1) measured these quantities for the supply air. Along the absorber length (item 6), 4 points were designed to allow air to be removed from the absorber at shorter distances. Only one connection is shown in Fig. 2, corresponding to a 67.5 cm contact length measurement, the longest possible run. These points were adjustable by using manual valves positioned at 10, 47.5, 57.5, and 67.5 cm from the air inlet in the case of a parallel flow, and at 10, 20, 57.5, and 67.5 cm for a counter flow configuration. Such a setup could divert the air to measure RH and T of air leaving the absorber as a function of contact length. Whichever contact length was chosen for a measurement, an airflow sensor was also placed after the T and RH sensor, as shown in Fig. 2 with points 4 and 5. As mentioned previously, these points were movable by connecting to any of the manually operated valves along the overall 67.5 cm absorber length. By changing the point where air enters the shell, we were able to change between parallel and counterflow configurations.

2.5. Air dehumidification experimental procedures

Previous work by our group studying a batch of desiccant in an open beaker has confirmed that faster absorption kinetics were obtained when a fixed quantity of desiccant is stirred: In the stirred case, surface absorption becomes limited by slower bulk diffusion rates of water into the desiccant, creating a saturated boundary layer at the air/desiccant interface [18]. That previous work is furthered here by using a membrane to contain the desiccant. The membrane has high water affinity that absorbs and transports water with kinetics much higher than the desiccant bulk diffusion, thereby not limiting the desiccant dehumidification capabilities.

2.5.1. Mass transfer of water vapor through membrane into non-flowing, neat desiccant

In the first experiment non-flowing desiccant of known state was evaluated inside the membrane shell and tube system in order to understand the basic membrane-desiccant interaction. Ambient air and neat liquid desiccant were run through the membrane system for 1 h to bring the system into steady state. The desiccant was pumped into the system at 0.012 mL/s. During this process,

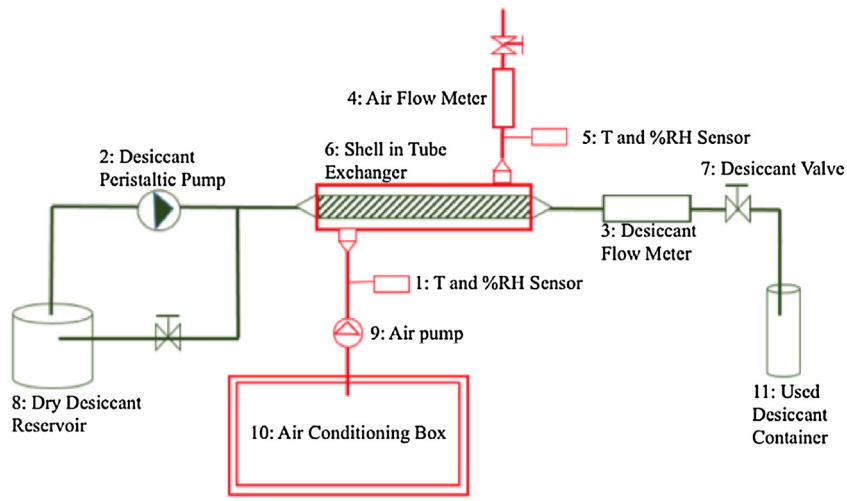

Fig. 2. Schematics of the experimental setup.

air that was in between membrane and shell of the exchanger was dehumidified to RH below 20%. This minimized water vapor pressure of the air surrounding the membrane, and significantly reduced the interaction of water molecules with the liquid desiccant molecules in contact with the Pebax® membrane before the experiment started.

Next, humid air was directed into the membrane exchanger, the liquid desiccant pump was stopped, and the valve connecting the peristaltic pump and the membrane was closed. Air conditioned to $T = 24\,^{\circ}C$ and RH = 80% with a flow rate of 1 L/min was then run through the membrane exchanger. T and RH of air was measured before it entered the exchanger, and immediately after it exited the absorber, after 67 cm. Airflow was measured after the air exited the exchanger.

2.5.2. Investigation of dehumidification rates at various liquid desiccant flow rates

This experiment was designed to measure the impact of liquid desiccant flow rate on air dehumidification in the absorber. The liquid desiccant flow rates were 0.005, 0.012 and 0.133 mL/s. The air flow was conditioned to $T = 25\,^{\circ}C$ and RH = 80%, and run through the membrane exchanger with flow rates of 0.5 and 1 L/min for each of the desiccant flows. T and RH of air was measured before it entered the exchanger and immediately after it went out of the exchanger. Although all the desiccant flow rates were kept in the laminar regime due to the high viscosity of the fluid, they represent an order of magnitude increase between each other.

2.5.3. Variation of air flow rate, shell size, flow arrangement, contact length, and specific humidity

This experiment studied a range of air conditions and flow. It represented the bulk of the work because changes in air conditions help characterize the range of mass transport kinetics indicating dehumidification potential of the system. The results are key for future work optimizing dehumidification rates in building-scale membrane-exchanger designs.

To normalize airflow rates across different volumetric flow rates and outer tube diameters, the Reynolds number (Re), was calculated using a hydraulic diameter of $D_H = D_o - D_i$, the kinematic viscosity of air, and the average cross-sectional air velocity given by the volumetric flow rate divided by the cross sectional area. These values along with the corresponding Re numbers are given in Table 1. The air flow rates used in the experiments were 0.035, 0.15, 0.5, 1 and 2 L/min. These air flows corresponded to velocities ranging from 0.017 to 13.47 m/s depending on the shell diameter, and Re was in the range from 5 up to 571 (Table 1). The shell sizes used were 1/8, 1/4, and 5/16 inch nominally, or 3.2, 6.4, and 7.9 mm actual ID, respectively, as mentioned in Section 2.4. The air was conditioned to have humidity ratios of 15 ($T = 24\,^{\circ}C$, RH = 80%), 20 ($T = 28\,^{\circ}C$, RH = 84%) and 25 g/kg ($T = 32\,^{\circ}C$, RH = 82%). For all of these conditions i.e., 5 flow rates, 3 shell sizes, and 3 specific humidity conditions, both counterflow and parallel flow setups were monitored at 4 different contact lengths. As to not change the experimental setup, these contact lengths were different for parallel flow and counterflow, and were given in Section 2.4.

For each combination of tube geometry, flow rate, and combination of air temperature and humidity, the temperature and humidity of the air entering and exiting the membrane exchanger were measured. The air side mass balance calculation was performed to quantify amount of moisture removed from the air by the desiccant. Results were reported as absolute humidity removed in g H_2O/kg air. Based on the contact length and diameter of the membrane, removed water vapor mass flux per unit area of membrane/desiccant surface area was calculated. The results were then used to compare the impact of different parameters.

Finally, we calculated the ε-NTU (Effectiveness-Number of Transfer Units) characteristics of the mass and heat exchanger using contemporary methods [29]. This was calculated after the kinetics experiments, and the shell and tube system geometry that can influence these results was not investigated. Therefore, these results indicate one potential performance, and future work will involve methods to investigate a full scale exchanger design. For the calculations, the precise form of the latent NTU, NTU_L, is given in Eq. (1), where ρ_a is the density of air in kg/m^3, $\dot{n}_\omega$ is the moisture flux in g_{water}/s, $\Delta C_{\omega,lm}$ is the log-mean concentration difference (similar to a log mean temperature difference from heat transfer) [7], and $\dot{m}_a$ is the air flow rate in kg_{air}/s. The full derivation of effectiveness and NTU is provided in the supplemental material file.

$$NTU_L = \frac{\rho_a \dot{n}_\omega}{\Delta C_{\omega,lm} \dot{m}_a} \tag{1}$$

3. Results and discussion

3.1. Mass transfer of water vapor through membrane into non-flowing neat desiccant

Previous work conducted by our group [18] indicated a diffusion-limited absorption rate. As the surface became more concentrated, if the vessel was not mixed, absorption rates slowed as

Table 1
Reynolds number (*Re*), calculations in bold for 15 flow configurations.

Pebax® tube OD (mm)	1.5	*Re* calculation				
Pebax® tube ID (mm)	1.1	Air flow rate (mL/min)				
Nominal ID (in.)	Actual ID (mm)	35	150	500	1000	2000
1/8	3.2	**10**	**43**	**143**	**286**	**571**
1/4	6.4	**6**	**26**	**85**	**170**	**341**
5/16	7.9	**5**	**22**	**72**	**143**	**287**

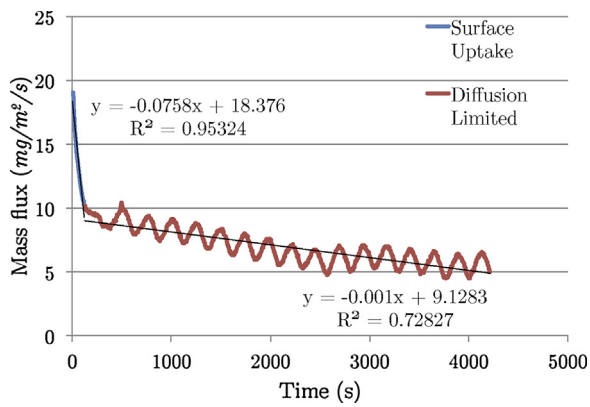

Fig. 3. Membrane moisture uptake (blue) followed by desiccant diffusion limited moisture uptake (red). The oscillations in the diffusion limited regime (red) are caused by the humidity sources control algorithm. (For interpretation of the references to color in this figure legend, the reader is referred to the web version of the article.)

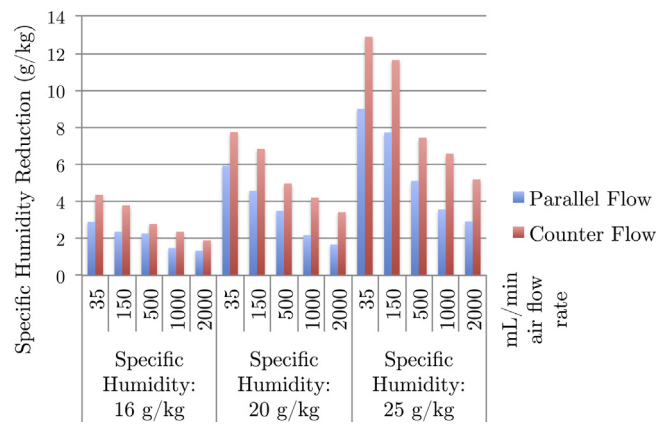

Fig. 4. Water vapor mass flux for different liquid desiccant flow rates in a 1/4 in. tube. The flow rates on the abscissa are given in mL/min, and the specific humidity in g/kg is for the supply air.

the system entered a diffusion limited regime. Water mass transport from the air onto the surface of the liquid desiccant is very fast compared to the diffusion from the surface of the desiccant down into the bulk material. Consequently, once the desiccant free surface is saturated, the dehumidification rate slows down considerably [18].

Fig. 3 summarizes the new findings for absorption through the Pebax® membrane, rather than from a free surface. The first regime starts with a very high flux that decays rapidly as the surface gets saturated. The second regime, with much slower mass flux decay, starts when surface is fully saturated and mass flux has become diffusion limited because water molecules arriving from the membrane no longer have abundant sites to sorb into, and they must wait for molecules in the saturated surface to diffuse down into the bulk desiccant. In the diffusion limited regime, shown in red in Fig. 3, the diffusion of water into the bulk desiccant becomes the limiting factor, as opposed to the blue regime where the unsaturated surface sorption is more favorable.

Previous work from our group [24] demonstrated that water vapor transport rates of 0.1 g/m^2/s through the Pebax® membrane was almost an order of magnitude higher than the fastest absorption rates (0.02 g/m^2/s) shown in Fig. 3. Since this type of mass transfer mechanism is often viewed as a resistance in series mechanism, the mass transfer through the membrane can be neglected beyond the membrane uptake regime. Using the standard resistance in series approach to mass transfer, diffusion of moisture into the desiccant acts as the large resistor in this scenario, thereby becoming the limiting rate once the front of water has reached the desiccant and saturated the membrane/desiccant interface.

The equilibrium membrane weight in different relative humidity environments was measured. The uptake was 1.1 g at 60% RH and 1.35 g at 80% RH. These are significant quantities, so ensuring equilibrium is important. Still, at the rates described above, the membrane would be at equilibrium on the order of minutes across the humidity ranges we were using even if a completely dry membrane was being used.

3.2. Variation of liquid desiccant flow rate

Results in Table 2 show the humidity ratio difference between air entering and exiting the membrane exchanger as a function of liquid desiccant and air flow rates. The liquid desiccant volumetric flow rates of 0.005, 0.012 and 0.133 mL/s correspond to desiccant velocities of 0.008, 0.064 and 0.2 m/s, respectively. The liquid desiccant flow was in the laminar regime for all examined flow rates, *Re* = 0.4, 3.3, and 10.3, respectively. Results indicate that an increase in the liquid desiccant flow rate by 2 orders of magnitude resulted in air dehumidification increase in the range of only 10.6 to 22.0% depending on the length of the membrane exchanger and airflow rate.

The increased water vapor removal of 10.6 to 22.0% can be observed when the liquid desiccant volumetric flow is increased from 0.005 to 0.133 mL/s. These results demonstrate that moisture uptake rates are directly related but largely unaffected by the desiccant flow rate because the non-negligible viscosity of the desiccant creates a thick boundary layer. Consequently, the boundary layer will not vary much for a large change in desiccant flow rate.

As shown in Table 2, two orders of magnitude increase in desiccant flow rate results in minor changes in the moisture uptake by the desiccant. For this reason, a constant desiccant flow rate of 0.012 mL/s was used for all subsequent experiments.

3.3. Counterflow vs. parallel flow configurations

As outlined in the Section 2, for each air flow rate, the inlet humidity ratio, and tube diameter were examined for the parallel and counterflow arrangements (see Fig. 4). As expected, for a given air and tube conditions, the counterflow setup outperforms the parallel one, because counterflow maintains higher concentration difference throughout the exchanger. For each data point in Fig. 4,

Table 2
Dehumidification measured in the humidity ratio reduction (bolded values) under various liquid desiccant flow rates and air flow rates, with calculated pressure drop through the desiccant tube.

				Air flow rate (L/min)			
Contact length (cm)	Desiccant flow rate (mL/s)	*Re*	Pressure drop (Pa)	0.5	Increase	1.0	Increase
10	0.005	0.4	1800	**1.23**	n/a	**1.03**	n/a
10	0.012	3.3	7600	**1.36**	10.6%	**1.14**	10.7%
10	0.133	10.3	48,300	**1.50**	22.0%	**1.24**	20.4%
67.5	0.005	0.4	12,300	**2.78**	n/a	**2.02**	n/a
67.5	0.012	3.3	51,500	**3.09**	11.2%	**2.29**	13.4%
67.5	0.133	10.3	326,000	**3.22**	15.8%	**2.41**	19.3%

counterflow demonstrates the biggest difference between the inlet air and exiting air. To avoid redundancy in data, only counterflow data is presented in subsequent sections.

3.4. Performance of counterflow configuration for different air conditions and membrane exchanger geometry

Results in Fig. 5 show relationship between dehumidification ability and air flow rate for three shell sizes. Dehumidification ability is presented as the absolute humidity reduction between air entering and exiting the membrane exchanger (Δg). The results indicate a strong influence of the air conditions and the physical characteristics of the membrane on (Δg), and they can be summarized as follows:

- Δg increases with the specific humidity of air entering the membrane exchanger.
- Δg decreases as the airflow rate increases.
- Δg augments with the length of the membrane exchanger.
- Δg goes down as the shell outer diameter increases.

Based on the removal of water from the air side, the desiccant utilization is calculated to range up to 0.012 g of water per gram of desiccant. Although this is small, the geometry and rate of uptake allow for rapid removal. Although the desiccant is not absorbing a large quantity of water, it is doing so rapidly enough that in relatively short lengths significant absolute humidity is removed. Generally more than 5 g/kg is removed in Fig. 5, which is enough for nominal removal in a majority of climates. For the most humid climates, the right of Fig. 5 shows removal above 10 g/kg bringing absolute humidity of tropical climates below 15 g/kg, adequate for maintaining less than 70% RH for 22 °C air conditions.

More importantly from a design perspective, when dehumidification is compared for different lengths of the membrane exchanger (Fig. 5), between 40 and 77% of the dehumidification takes place during the first 10 cm of the exchanger. This can also be noted in Fig. 3 where the 10 cm moisture removal is nearly half of the six times longer 67.5 cm removal. The results show that the initial 10 cm of the membrane are much better utilized than the last 57 cm of the total length.

This can be attributed to the diffusion limited mass transfer as shown in Fig. 3 with no desiccant flow. In the scenario with flowing desiccant, unsaturated desiccant enters the system at $x = 0$ cm, the partial pressure difference of moisture in the air, and moisture in the desiccant is highest when the vapor pressure of moisture in the desiccant is nearly 0. Since diffusion of moisture through the desiccant is slower than absorption into dry desiccant, the initially large partial pressure difference decays quickly since moisture does not diffuse into the bulk desiccant fast enough. As a consequence, the large difference of partial pressure between the air and desiccant surface inside the tube is greatly reduced. The absence of mixing of the desiccant results in water saturation only on the surface of the desiccant, which yields a diffusion limited absorption process. Due to constraints with the tube dimensions, data from increments less than 10 cm could not be acquired. The effect of shell size indicates that smaller diameters provide more intensive water vapor exchange per unit of area and time as the smaller diameter increases the *Re* number.

Results from Fig. 6 for counter flow show that higher *Re* numbers lead to an increase in moisture mass flux exchange in the laminar regime, and confirm that the highest rates occur in the first part of the exchanger. The moisture mass flux is highest for the smallest diameter of the membrane exchanger shell (increasing *Re*), assuming all other parameters constant, therefore Fig. 6 shows data only from the smallest 3.2 mm shell. As shown in Fig. 6, the highest moisture mass flux is achieved with the highest airflow rates (highest *Re*). (Additional experimental data acquired under identical conditions for shell diameters of 6.4 and 7.9 mm are available in Supplemental Material file.)

When comparing Fig. 6a–c, one notices the supply air specific humidity of 16, 20, and 25 g/kg, all maintain an 80% RH. Since the activity, or %RH, difference between the moisture in the air and desiccant is the driving force for absorption, this driving force decays faster at lower specific humidities. Such a trend is observed in Fig. 6a–c. In Fig. 6a, the 10 and 20 cm lengths are nearly indistinguishable in terms of the moisture mass flux observed. This is because after 10 cm, the driving force decreases quickly, and the small quantity of moisture being removed has not yet saturated the surface sites available for absorption at the membrane/desiccant interface. As opposed to Fig. 6b and c, by 20 cm there is already a markedly diminished mass flux. The transition to being diffusion limited now occurs before 20 cm of contact length, rather than what is shown in Fig. 6a, where the diffusion limited regime is approached somewhere between 20 and 57.5 cm of contact length.

The data follow the general convective transport rule where the mass transfer, *K*, is proportional to *Re* raised to a nonunity power. Such an analysis is typical for heat transfer, but can also be extended to mass transfer. Mass transfer rate is a function of mass diffusivity, characteristic length, and Sherwood number (often referred to as the mass transfer Nusselt number, which is related to *Re* and Schmidt number). The trend indicates that higher *Re* flow would result in higher mass transfer, something that could be accomplished by reducing the air side tube's diameter for a fixed volumetric flow rate, thereby reducing the proportion of air volume to boundary layer volume.

Figs. 5 and 6 appear to be inverted, with Fig. 5 showing greater absolute humidity reduction for low air flow rates, and Fig. 6 showing the greater mass flux for higher air flow rates (higher *Re*). This is because low flow rates correspond to less air being supplied, so when calculating the overall mass flux, higher flow rates correspond to greater mass flux despite having a higher relative humidity when exiting the contacter. The two charts convey information useful for different purposes. For instance, Fig. 5 would be used for sizing a system based on a desired specific humidity reduction. Tubes could be placed in parallel to achieve the necessary flow rate, all from information obtained on the chart. Fig. 6 is

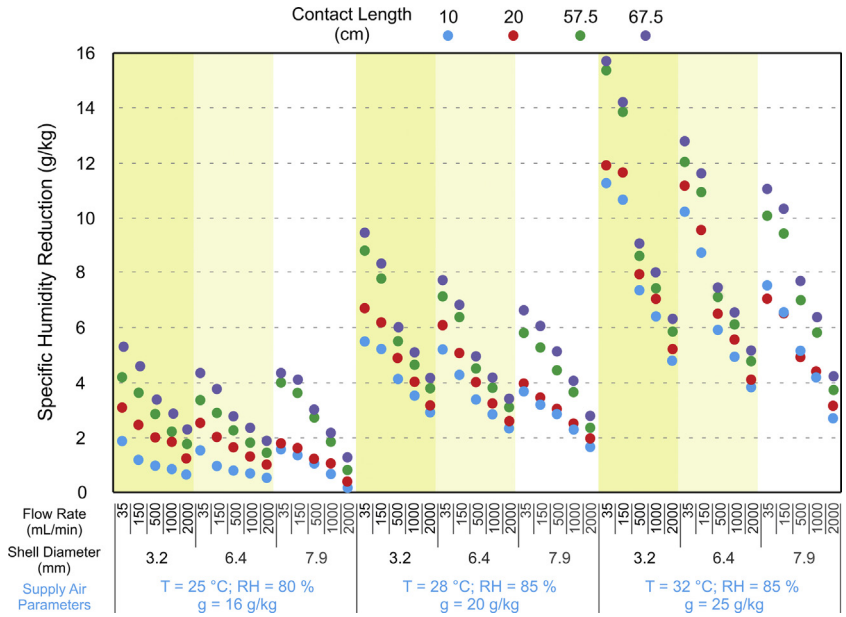

Fig. 5. Absolute humidity reduction for flow configurations at varying air flow rates and contact lengths for brackets of supply humidity experimental conditions.

useful for understanding the physical basis of the system from a fundamentals perspective.

3.5. Volume utilization of liquid desiccant in counter flow configuration

Fig. 7 illustrates the relationship between measured *Re* of the airflow for all studied contact lengths and the (a) desiccant utilization, and (b) utilization normalized per unit contact length. The value for utilization reaches a maximum at 0.012 $g_{water}/g_{desiccant}$. This emphasizes that an increase in contact time between the dehumidifying surface and humid air, due to the lower velocity inside the shell, has a smaller impact than a combined increase in mass transfer coefficient and *Re*. Additionally, for a given airflow rate, mass flux is higher for the smaller shell diameter.

However, simply designing a system for only high volume utilization neglects other important parameters. While Fig. 7a shows more utilization of the desiccant on a $g_{water}/g_{desiccant}$ basis after longer contact length as would be expected, Fig. 7b shows how the rate of uptake suffers at longer lengths. As shown in Table 2, longer contact lengths yield higher pressure drops, so when viewed in conjunction with Fig. 7b, there is a clear tradeoff between pressure drop inside the desiccant tube and mass transfer rate. Since the mass transfer rate decreases so rapidly, this data shows how important it would be in terms of parasitic power to design a system with short contact lengths to maximize parasitic power per g_{water} absorbed. Additionally in Fig. 7b, there are two discontinuous zones on the right side, which are artifacts of the contour plot of the discrete data, but indicates a tendency toward constant change in utilization per unit contact length for the high *Re* and longer contact lengths where bulk diffusion limits would dominate.

Each contact length corresponds to a pressure drop (reported in Table 2) for the desiccant flowing in the interior tube. Multiplying the pressure drop to the volumetric flow rate of the desiccant gives a theoretical pumping power as a function of contact length. The data reported in Fig. 7a was multiplied by desiccant flow rate, and this number was divided into the theoretical pumping power for each contact length, yielding an energy demand per gram of water removed. The results were plotted in Fig. 8. As expected, because of the high pressure drop at longer contact lengths and the poor desiccant utilization at longer lengths and low Re_{air}, it is very costly in terms of energy demand to remove water in such a regime. Because of the faster absorption kinetics in the first 10 cm, this is the range in which it is most efficient to remove moisture. These values compare favorably to other work [8], with the best energy per water removal rate in our system at 1.5 J/g_{water} comparing to 54 J/g_{water} for LiCl systems. Despite the anticipated high air side pressure drop in a scaled up version of our system, the low parasitic power of the desiccant side is a promising takeaway providing future designs the ability to sacrifice air side efficiency if required.

Using the ε-NTU method to assess system performance, we calculated a maximum NTU_L of 8.5 which corresponded to 16 g/kg supply air at 35 mL/min after 67.5 cm of contact length, which had a corresponding latent effectiveness, ε_L, of 0.08. The highest latent effectiveness measure was 0.58, occurring at an air flow 35 mL/min, 25 g/kg supply air after 10 cm of contact length, corresponding to NTU_L of 0.17. Both data points occurred in the small 3.2 mm supply air tube. When cross-referenced with Fig. 8, these data both correspond to values for $Re_{air} = 10$, which corresponds to at least 50 J/g_{water}. Therefore, when considering the system with a reference to pumping costs, the data shows a clear tradeoff between ε_L, NTU_L, and desiccant pumping power. This tradeoff informs future work which aims to increase effectiveness using geometric solutions to keep pumping costs low by encouraging mixing through additional means.

4. Potential applications

Fig. 7 provides insights into how our system would be applicable for a room requiring humidity removal. For instance, a membrane desiccant dehumidification system based on our analysis could be designed with short exchange lengths between mixing components for disturbing the desiccant boundary layer, which would exhibit larger overall uptakes (active dehumidification) than a single and continuous, straight reactor of the same length. This is because the diffusion limited regime is reached quickly (within 10 cm domain), and mixing could generate a new unsaturated layer of desiccant at the membrane-desiccant interface maintaining fast surface uptake in Fig. 3 and better uptake per unit length as shown in Fig. 7b. Future studies will seek to characterize this domain with greater resolution.

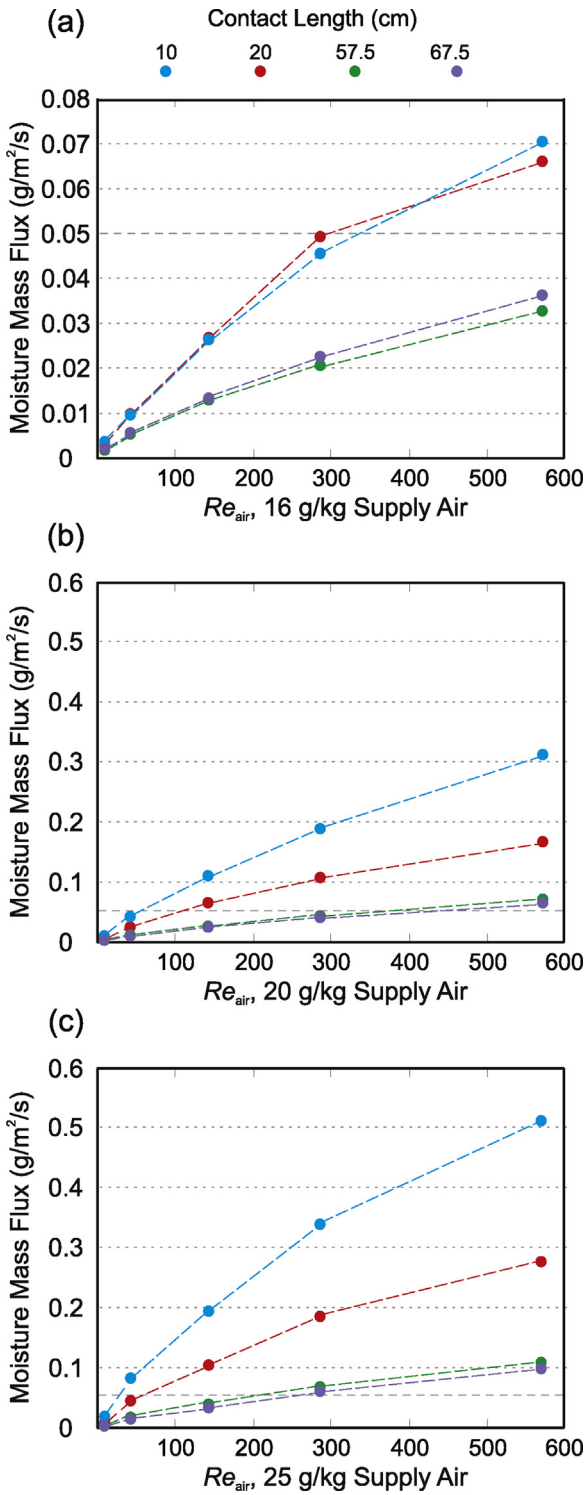

Fig. 6. Water vapor mass flux for flow configurations at varying *Re* for brackets of supply humidity experimental conditions, and outer shell diameter of 3.2 mm.

A major takeaway from our study is an improved understanding of not only the behavior, but also the limiting factors of the shell-tube exchanger configuration. In particular, we carried out an in-depth study on: the absorption rate relationships using air flow, humidity, and geometry as independent variables. All of this information is important when designing equipment for future studies or pilot installations. Liquid desiccant systems have the potential to be miniaturized, and therefore, to be easily integrated into mechanical systems and building components, like facade and floor slabs. They may provide considerable savings in terms of space, materials, and energy [20]. They also enable the operation of radiant cooling systems with the highest, and most energy efficient temperatures, without the need for any supplementary low-temperature mechanical dehumidification. Instead of requiring these additional low-temperatures, the desiccant can operate using waste heat to drive the dehumidification process, and allow the sensible cooling to be delivered with the highest possible system performance.

In addition, the ε-NTU analysis available in the Supplemental Material file provides preliminary insights to our work in terms of device engineering. While the motivation for this work was centered around the kinetics and chemical interactions between the nonporous hydrophilic membrane and the desiccant, and not a full-scale exchanger design, the trade-off that emerged between pumping power and ε_L and NTU_L value and pumping energy demand can certainly be used to inform future system optimization. In a future study, we will investigate in detail the performance aspect of the mass exchanger with appropriate experimental setups, addressing desiccant utilization effectiveness as related to the system geometry to promote desiccant mixing and reduce pumping in a diffusion limited regime.

In order to consider an example of decentralized system application, the membrane system is scaled up for 10 private offices each with a surface area of 12 m^2. The offices are assumed to be in a climate that requires dehumidification of outdoor air from 22 to 10 g/kg. Outdoor air demand for these offices and their occupants are based on ASHRAE 62.1 at 61 L/s. To quantify this system, interpolating data points from Fig. 5 shows that for a 22 g/kg inlet air condition, a 10 cm tube with a flow rate of 2L/min would provide approximately 4.5 g/kg in absolute dehumidification. To reach the desired 61 L/s, dividing this by 2 L/min yields 1830 tubes. To achieve the desired 10 g/kg incoming air setpoint, these tubes would have to be organized in series 3 times, ideally with two mixing stages between the three contacter. The contact area can thus be packed in the membrane exchanger with dimensions of 0.27 m × 0.27 m × 0.4 m (h × W × L), using individual shell in tube units that are 6 cm × 6 cm. This is a very promising initial estimation of potential system embodiment that can be further optimized. Compared to recent research by Oh. et al. for desiccant dehumidification in the tropics [17], the results from our initial alkoxylated siloxane experimental setup can remove the same and often more moisture from humid supply air.

Additionally, the modified silicone oil that comprises the alkoxylated siloxane desiccant behaves as a type III desiccant [15]. Type III desiccants have near exponentially increasing saturation equilibrium points with increasing activity, or relative humidity, of water in the supply air. The saturation equilibrium dependence on activity means removing the water from the desiccant during regeneration becomes comparatively easy, as a known issue with LiCl, a type I desiccant, is the heat required for regeneration. Dry exhaust air can be heated to 50 °C for regeneration, which is not required for the heat but instead just to drop the relative humidity of the air. Therefore, regeneration can be more easily achieved without substantial heating of the desiccant, which will be analyzed in subsequent experiments of the membrane desiccant system.

Scaling up such a system would require careful consideration of air flow rate and contact length. For instance, a comparison between Figs. 5 and 6, highlights the tradeoff between absolute humidity removal and mass flux. The trend in Fig. 5 implies that longer pipes will provide increasing humidity removal, at diminishing returns. Naturally, such a scenario is not optimal from a viscous fluid pumping perspective. While the numbers in this study should be taken as a starting point when designing a system for a required humidity removal, it is important to introduce a mixing stage after 10 cm of contact length. Additionally, Fig. 7 shows the saturation of the desiccant as a function of contact length, and

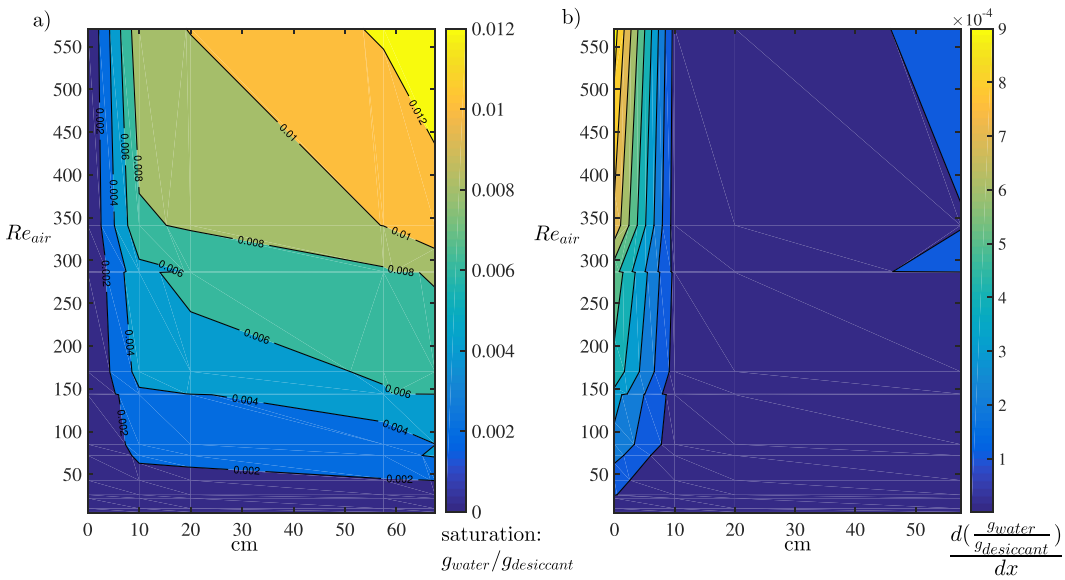

Fig. 7. (a) Utilization of desiccant with water vapor as a function of contact distance and *Re* for counterflow experiments (grams of water per gram of desiccant). (b) Change in utilization per unit length (cm) of Fig. 7a.

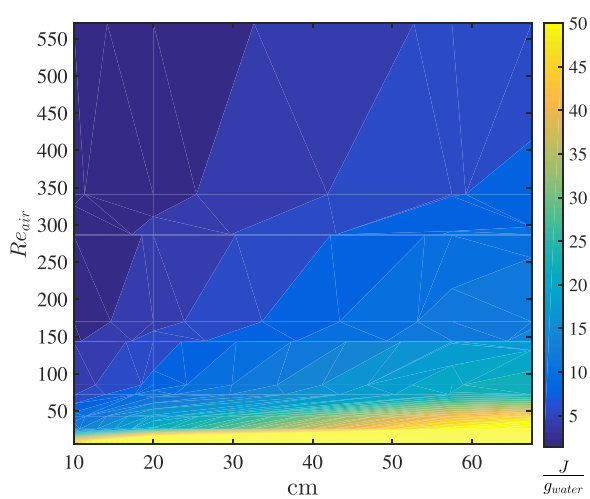

Fig. 8. The calculated pumping demand for dehumidification in joules, *J*, per gram of water moved from the air to the desiccant. The values range from min 1.5 to max 250.0 J/g_{water}, not shown fully on the color scale.

in no configuration is the bulk saturation high after 10 cm. This is a key information in terms of regeneration efficiency perspective, as another source of inefficiency would be the energy used to pump the insufficiently saturated desiccant that requires regeneration. Therefore, a design for only high mass flux comprising a single 10 cm exchanger with as many separate tubes as demonstrated in this study would not be desirable either. Taking into account two independent design variables such as, the required airflow volume, and the absolute humidity removal, we may scale up our system by taking the following optimal absorption criteria: (i) approximately *Re* 500 airflow, (ii) approximately 10 cm of contact length, which corresponds to approximately 6 g/kg of absolute humidity removal and 0.31 g/m^2/s of mass flux for a single tube. A set of tubes could be placed in an array to meet the desired ventilation rate, and repeated in series to obtain the required absolute humidity reduction for the design parameters.

The Pebax® membrane chosen for the mass exchanger material not only ensures separation of the desiccant air stream delivered to the building (from absorber) or environment (from desorber), but it also does not restrict the mass transfer from the humid air to the desiccant. The measured mass transfer rate per square meter of Pebax® measured by Teitelbaum et al. [24] is an order of magnitude higher than the absorption per square meter of desiccant being continuously stirred in a beaker [18], demonstrating that the rate limiting step is the absorption of moisture into the desiccant. A possible limitation might be the mechanical stability of the membrane and its ability to withstand long working hours, because the hydrophilic membrane absorbs water molecules from the surrounding environment and elongates during operation. Future experiments are intended to quantify the presence of elastic and plastic deformations in the polymeric membrane.

5. Conclusions

In this work, we have described and evaluated a prototype liquid desiccant absorber that addresses several problems encountered in these types of devices. Our conclusions are summarized below:

- The use of a noncorrosive liquid desiccant eliminates the need for expensive metal parts (e.g., titanium).
- Carryover problem was solved by physically separating air and liquid desiccant stream with nonporous hydrophilic membrane, which has negligible mass transfer resistance.
- A counterflow setup is a more effective mass exchanger than a parallel one.
- Moisture removal was weakly dependent on desiccant flow rate due to a persistent laminar boundary layer pumping power can be minimized while maintaining reasonable performance.
- The humidity ratio of the air entering the membrane system was reduced by up to 15.7 g of water per kg dry air, and the maximum latent NTU and effectiveness were 8.5 and 0.08 respectively.
- Desiccant utilization in the system went up to 0.012 g of water per gram of desiccant, which is relatively small, but typical for this type III desiccant where we are interested in high system kinetics instead of capacity.
- The system demonstrates very rapid kinetics, up to 0.5 g/m^2/s, of moisture uptake in the initial contact between the air stream and the desiccant.
- Between 40 and 77% of the dehumidification takes place within the first 10 cm of the air–liquid desiccant contact zone. This result

shows the importance of the first region where contact surface is not saturated with bonded molecules, and informs design opportunities to re-mix and maintain highly effective moisture removal.

The conclusions above indicate the direction of future work to further investigate the hypotheses developed in this study for system performance, and to support development of a larger multi-stage moisture removal system. We will further address this rapid reduction of the absorption kinetics after the first 10 cm of contact length, by following two directions: (i) fully characterize the rapid uptake kinetics within the 10 cm region, and (ii) improve overall kinetics by favoring access to the bulk desiccant surface through mixing, and considering even higher *Re*. Auxiliary power calculations for fan power will also be added to the desiccant power calculations. The regeneration ability also needs to be experimentally confirmed with various air temperatures and humidities, and desiccant temperatures and water saturation. The hypothesized surface versus bulk diffusion challenge could be expected for the regeneration operation as well, where the surface releases water molecules quickly and bulk diffusion must be mitigated with mixing. In addition we will consider new methods to accurately quantify water traces in the desiccant by developing a gas chromatography protocol or by using a Karl Fischer titration method. Finally, we aim to build room-scale prototypes to enable high-temperature radiant and passive chilled beam cooling systems without the need for additional mechanical dehumidification, thereby addressing the significant challenge of cooling demand in hot and humid climates where many of the largest developing cities are located.

Acknowledgements

The authors acknowledge financial support through the E-ffiliates program at Princeton University's Andlinger Center for Energy and the Environment. The authors wish to thank Christopher Bertelo, Mark Aubart and Nicholas Deluca from Arkema Inc. (King of Prussia, PA); Dongchan (Shaun) Ahn, and Aaron Greiner from Dow Corning Corp. (Midland, MI). We also thank Prof. Jay Benziger for pertinent discussions. Additionally, we would like to thank Indira Roy for her contributions with calculations and graphics in the supplemental material.

Appendix A. Supplementary data

Supplementary data associated with this article can be found, in the online version, at https://doi.org/10.1016/j.enbuild.2017.10.093.

References

[1] C.S. Khalid Ahmed, P. Gandhidasan, S.M. Zubair, A.A. Al-Farayedhi, Exergy analysis of a liquid-desiccant-based, hybrid air-conditioning system, Energy 23 (1) (1998) 51–59.
[2] D. Ahn, A. Greiner, J. Hrabal, A. Lichtor. Method of separating a gas using at least one membrane in contact with an organosilicon fluid, September 25 2013. US Patent App. 14/413,231.
[3] A. Baughman, E.A. Arens, Indoor humidity and human health – Part I: Literature review of health effects of humidity-influenced indoor pollutants, ASHRAE Trans. 102 (1996).
[4] S. Bergero, A. Chiari, Experimental and theoretical analysis of air humidification/dehumidification processes using hydrophobic capillary contactors, Appl. Therm. Eng. 21 (11) (2001) 1119–1135.
[5] S. Bergero, A. Chiari, Performance analysis of a liquid desiccant and membrane contactor hybrid air-conditioning system, Energy Build. 42 (11) (2010) 1976–1986.
[6] R.S. Das, S. Jain, Experimental performance of indirect air–liquid membrane contactors for liquid desiccant cooling systems, Energy 57 (2013) 319–325.
[7] A. Gabelman, S.-T. Hwang, Hollow fiber membrane contactors, J. Membr. Sci. 159 (1) (1999) 61–106.
[8] K. Gommed, G. Grossman, Experimental investigation of a liquid desiccant system for solar cooling and dehumidification, Sol. Energy 81 (1) (2007) 131–138.
[9] L.G. Harriman III, D. Plager, D. Kosar, Dehumidification and cooling loads from ventilation air, ASHRAE J. 39 (11) (1997) 37.
[10] S.-M. Huang, L.-Z. Zhang, Researches and trends in membrane-based liquid desiccant air dehumidification, Renew. Sustain. Energy Rev. 28 (2013) 425–440.
[11] A. Ito, Dehumidification of air by a hygroscopic liquid membrane supported on surface of a hydrophobic microporous membrane, J. Membr. Sci. 175 (1) (2000) 35–42.
[12] K. Kneifel, S. Nowak, W. Albrecht, R. Hilke, R. Just, K.-V. Peinemann, Hollow fiber membrane contactor for air humidity control: modules and membranes, J. Membr. Sci. 276 (1) (2006) 241–251.
[13] A. Lowenstein, Review of liquid desiccant technology for HVAC applications, HVAC & R Res. 14 (6) (2008) 819–839.
[14] F. Meggers, J. Pantelic, L. Baldini, E.M. Saber, M.K. Kim, Evaluating and adapting low exergy systems with decentralized ventilation for tropical climates, Energy Build. 67 (2013) 559–567.
[15] S.A. Mumma, DOAS and desiccants, Eng. Syst. 24 (8) (2007) 37–38.
[16] R.G. Nevins, R.R. Gonzalez, Y. Nishi, A.P. Gagge, Effect of changes in ambient temperature and level of humidity on comfort and thermal sensations, ASHRAE Trans. 81 (2) (1975) 169–182.
[17] S.J. Oh, K.C. Ng, K. Thu, M.K. Ja, M.R. Islam, W. Chun, K.J.E. Chua, Studying the performance of a dehumidifier with adsorbent coated heat exchangers for tropical climate operations, Sci. Technol. Built Environ. 23 (1) (2017) 127–135.
[18] J. Pantelic, E. Teitelbaum, S. Kim, H. Guo, A. Schlueter, F. Meggers, Air dehumidification with novel liquid desiccant system, Expanding Boundaries: Systems Thinking for the Build Environment (2016).
[19] J. Potreck, K. Nijmeijer, T. Kosinski, M. Wessling, Mixed water vapor/gas transport through the rubbery polymer pebax® 1074, J. Membr. Sci. 338 (1) (2009) 11–16.
[20] A. Schlueter, A. Rysanek, C. Miller, J. Pantelic, F. Meggers, M. Mast, M. Bruelisauer, C.K. Wee, 3for2. Realizing spatial, material, and energy savings through integrated design, CTBUH J. 2 (2016).
[21] P. Scovazzo, J. Burgos, A. Hoehn, P. Todd, Hydrophilic membrane-based humidity control, J. Membr. Sci. 149 (1) (1998) 69–81.
[22] P. Scovazzo, A. Hoehn, P. Todd, Membrane porosity and hydrophilic membrane-based dehumidification performance, J. Membr. Sci. 167 (2) (2000) 217–225.
[23] Y. Shangguan, Intrinsic Properties of Poly (Ether-B-Amide)(Pebax® 1074) for Gas Permeation and Pervaporation, PhD thesis), University of Waterloo, 2011.
[24] E. Teitelbaum, F. Meggers, G. Scherer, P. Ramamurthy, L. Wang, E. Bou-Zeid, Eccentric buildings: evaporative cooling in constructed envelopes by transmission and retention inside casings of buildings, Energy Proc. 78 (2015) 1593–1598.
[25] H. Tsutsumi, S.-I. Tanabe, J. Harigaya, Y. Iguchi, G. Nakamura, Effect of humidity on human comfort and productivity after step changes from warm and humid environment, Build. Environ. 42 (12) (2007) 4034–4042.
[26] J. Martin Wimby, T.S. Berntsson, et al., Viscosity and density of aqueous-solutions of libr, licl, znbr2, cacl2, and lino3. 1. Single salt-solutions, J. Chem. Eng. Data 39 (1) (1994) 68–72.
[27] M. Yang, S.-M. Huang, X. Yang, Experimental investigations of a quasi-counter flow parallel-plate membrane contactor used for air humidification, Energy Build. 80 (2014) 640–644.
[28] L.-Z. Zhang, Fabrication of a lithium chloride solution based composite supported liquid membrane and its moisture permeation analysis, J. Membr. Sci. 276 (1) (2006) 91–100.
[29] L.-Z. Zhang, Conjugate Heat and Mass Transfer in Heat Mass Exchanger Ducts, Elsevier, 2014.
[30] L.-Z. Zhang, Y.-Y. Wang, C.-L. Wang, H. Xiang, Synthesis and characterization of a PVA/LICL blend membrane for air dehumidification, J. Membr. Sci. 308 (1) (2008) 198–206.